Soil Dynamics and Earthquake Engineering 144 (2021) 106677

Contents lists available at ScienceDirect

Soil Dynamics and Earthquake Engineering

journal homepage: http://www.elsevier.com/locate/soildyn

Assessment of the efficacies of correction procedures for multiple thin layer effects on Cone Penetration Tests

Kaleigh M. Yost [a], Russell A. Green [a,*], Sneha Upadhyaya [a], Brett W. Maurer [b], Alba Yerro-Colom [a], Eileen R. Martin [c], Jon Cooper [c]

[a] Department of Civil and Environmental Engineering, Virginia Tech, Blacksburg, VA, USA
[b] Department of Civil and Environmental Engineering, University of Washington, Seattle, WA, USA
[c] Department of Mathematics and Division of Computational Modeling and Data Analytics, Virginia Tech, Blacksburg, VA, USA

ARTICLE INFO

Keywords:
Cone penetration test (CPT)
Thin-layer correction
Liquefaction
Liquefaction potential index (LPI)
Earthquake
New Zealand

ABSTRACT

Multiple interbedded fine-grained layers in a sand deposit have a "smoothing" effect on the measured Cone Penetration Test (CPT) tip resistance (q_c), resulting in a significant underestimation of the predicted liquefaction resistance of the sand layers. Trends identified by De Lange [14] through calibration chamber tests on stratified sand-clay profiles are used herein to develop a new thin-layer correction procedure for q_c (the "Deltares" procedure). The efficacies of the Deltares and the independently-developed Boulanger and DeJong [6] procedures are both directly assessed using CPT data from calibration chamber tests and indirectly inferred from CPT-based liquefaction case histories in Christchurch, New Zealand. The results highlight limitations of the assessed thin-layer CPT q_c correction procedures for layers less than 40 mm thick. Multiple, interbedded thin layers also influence the measured CPT sleeve friction (f_s), but in a more complex way than they influence q_c. To-date, no procedures have been proposed to address all the thin-layer-effects phenomena on the measured f_s, with errors in properly characterizing the f_s of a layer inherently influencing the accuracy of predicting the liquefaction susceptibility and potential of the layer. In totality, the thin-layer-effects correction procedures proposed to-date generally result in slightly less accurate predictions of the observed liquefaction severity for cases having highly stratified profiles, opposite of what would be expected and desired.

1. Introduction

For over forty years, extensive research efforts have focused on developing procedures for evaluating liquefaction triggering, resulting in significant advances in the state-of-practice (e.g., Whitman [53]; Seed and Idriss [43]; Seed et al. [44]; Stark and Olson [45]; Robertson and Wride [41]; Youd et al. [54]; Andrus et al. [2]; Cetin et al. [11]; Moss et al. [36]; Idriss and Boulanger [25,26]; Kayen et al. [28]; Boulanger and Idriss [7]; Green et al. [22,23]; among others). The success of these efforts is highlighted by the relatively high accuracy of several currently-used liquefaction models (e.g., Green et al. [19,20]). However, the primary focus of past research was on liquefaction triggering of cohesionless, free-draining soil deposits and not on predicting the liquefaction response of soil profiles with complex stratigraphy, such as sand profiles with multiple interbedded silt and/or clay layers (Beyzaei et al. [5]). Comparison of predicted versus observed severity of surficial liquefaction manifestations at sites comprised of sand with interbedded silt and clay during the 2010–2011 Canterbury, New Zealand, earthquake sequence (CES) highlighted significant limitations in the predictive capabilities of current liquefaction triggering and/or manifestation models (e.g., Maurer et al. [29]). In general, current methods accurately predicted liquefaction severity in eastern Christchurch, but significantly over-predicted liquefaction severity in western Christchurch, particularly in southwest Christchurch.

In an effort to understand the reason for these trends in the geospatial prediction accuracy, Maurer et al. [30] computed the average Cone Penetration Test (CPT) Soil Behavior Type Index (I_c) (Robertson [39]) for the upper 10 m (I_{c10}) of profiles across Christchurch, where I_c is commonly used as a proxy for soil type and fines content (FC). Maurer et al. [30] observed that the deposits in eastern Christchurch predominantly have an $I_{c10} < 2.05$ and those in western Christchurch predominantly have an $I_{c10} > 2.05$, which is a direct result of the depositional environments of the respective deposits. Note that $I_c = 2.05$ separates "Sands" (i.e., clean sands to silty sands) from "Sand Mixtures" (i.e., silty

* Corresponding author.
E-mail address: rugreen@vt.edu (R.A. Green).

https://doi.org/10.1016/j.soildyn.2021.106677
Received 4 January 2021; Received in revised form 15 February 2021; Accepted 16 February 2021
Available online 1 March 2021

sand to sandy silt) (Robertson and Wride [42]).

Upon more detailed studies of the geologic, geomorphic, and geotechnical characteristics of the profiles that have an $I_{c10} > 2.05$, the profiles were shown to be highly stratified and composed of multiple thin soil layers (e.g., Beyzaei et al. [4]; Stringer et al. [46]; van Ballegooy et al. [50]; McLaughlin [35]; Beyzaei et al. [5]; Cox et al. [13]; among others). Boulanger et al. [8] noted the limitation of the CPT, as well as other in-situ tests commonly used to predict liquefaction triggering, to identify and characterize thin layers that may significantly influence the liquefaction response of a soil profile. Specifically, multiple interbedded layers have a "smoothing" effect on the measured CPT tip resistance (e.g., van der Linden [51]), generally resulting in a significant underestimation of the density of the sand layers and an overestimation of the stiffness of the fine-grained layers.

CPT tip resistance (q_c) measurements are made as a function of depth, usually in depth increments of one to 2 cm, and sometimes up to 5 cm. However, q_c is influenced by soil ~10–30 cone diameters ahead of the cone tip, with the zone of influence being smaller for looser/softer soils and larger for denser/stiffer soils (Ahmadi and Robertson [1]). As a result of this "stress-bulb-influence-zone" phenomenon, measured values of q_c reflect average values for the soils in the zone of influence and do not represent the "true" values for the soil at a given depth. This is conceptually illustrated in Fig. 1 which shows the influence of a sand layer of varying thickness on the measured tip resistance in a profile composed of both clay and sand strata. As shown, the measured q_c is influenced by the stiffer sand layer while the depth of the CPT tip is still in the overlying clay layer. Similarly, the measured q_c is also influenced by the underlying softer clay layer while the CPT tip is in the overlying sand layer. Also, the measured q_c for the sand layer is increasingly biased to be less than the fully developed or "true" q_c for the layer as the layer gets thinner. These phenomena are referred to as transition and thin-layer effects (e.g., Ahmadi and Robertson [1]). Deltares performed a series of calibration chamber tests on soil profiles consisting of thinly interlayered soft clay and sand of varying layer thicknesses and densities (De Lange [14]) that experimentally confirm these phenomena. The results showed that the measured q_c in the interbedded sand layers is less than the "true" q_c for the layers by a factor of 1.5–6, where the "true" q_c for the sand layers was determined by testing reference soil models consisting solely of sand of similar density.

The inability of the CPT to properly characterize highly stratified profiles for predicting liquefaction was highlighted by the CES. However, this shortcoming is of relevance to many other regions of the world, for example, the Flaser beds or tidal flats in the Groningen region of the Netherlands. Similar to the soil profiles in western Christchurch, these complex soil profiles are comprised of multiple thin layers of coarse and fine grained soils. The cost of mispredicting the liquefaction damage potential due to multiple thin-layer effects can be significant if soil improvement schemes are implemented to mitigate the erroneously high predicted liquefaction hazard, such as in the Hawke's Bay region of New Zealand (El Kortbawi et al. [15]).

Procedures have been proposed to correct q_c for "thin-layer effects" (e.g., Robertson and Fear [40]), but most of these procedures are manually implemented and are not able to correct for multiple thin layers that influence measured q_c at a given depth. However, Boulanger and DeJong [6] recently proposed an automated procedure to account for multiple thin-layer effects by posing it as an inverse problem, assuming the measured q_c is equal to the "true" q_c convolved with a depth-dependent spatial filter following a simple 1D model.

This paper aims to evaluate the efficacy of thin-layer correction procedures in terms of accuracy (i.e., the ability to estimate "true" q_c, as obtained in laboratory calibration chamber test data, from "measured" q_c) and the ability to reconcile erroneously high liquefaction predictions, particularly for soil profiles with very thin layers (less than 40-mm-thick). Towards this end, first, an overview of the De Lange [14] calibration chamber data is presented, followed by an overview of the Boulanger and DeJong [6] (BD18) inverse filtering procedure. The BD18 procedure is then modified in an attempt to improve its thin-layer correction abilities, with the modified procedure referred to as BD18MOD. A new procedure based on the Koppejan pile capacity method is then proposed, with this procedure referred to herein as "Deltares" procedure because it is derived from work presented in De Lange [14]. The efficacies of BD18, BD18MOD, and Deltares procedures are directly evaluated using the calibration chamber data, as well indirectly inferred from CPT-based liquefaction case history data from the Canterbury, New Zealand, earthquakes.

2. Overview of calibration chamber tests

As mentioned in the Introduction, Deltares performed a series of calibration chamber tests on pure sand and stratified sand-clay profiles to gain insights into the effect of multiple thin layers on measured q_c. Details about the calibration chamber tests are extensively presented in De Lange [14] and, thus, are only briefly summarized herein. The calibration chamber used was cylindrical in shape, and had an inner diameter of 0.9 m and a height of 0.96 m. The chamber was lined with a flexible rubber membrane, with a porous geotextile placed between the chamber wall and rubber membrane to allow water to flow into the annulus to control lateral pressure applied to the soil sample.

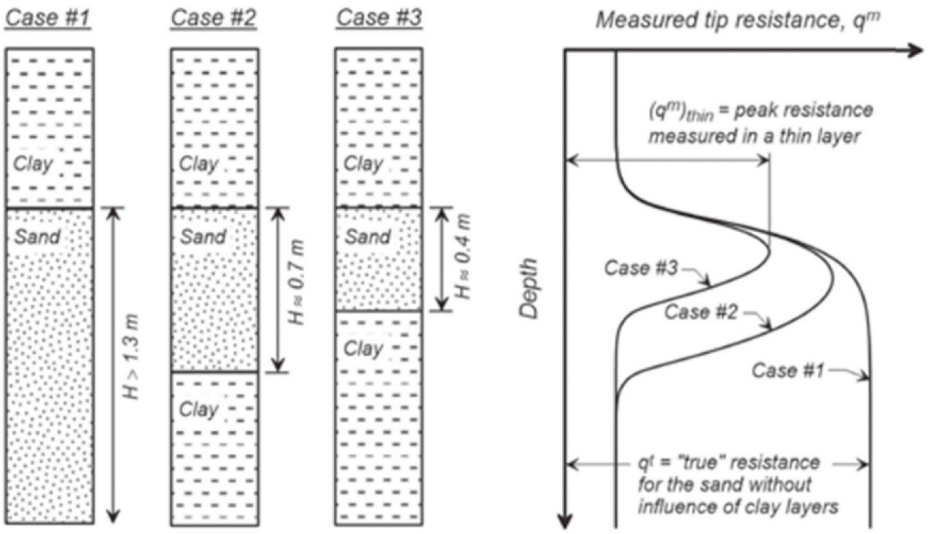

Fig. 1. Schematic of thin-layer effect for a sand layer of varying thickness embedded in a clay layer (Idriss and Boulanger [26]).

Additionally, a water-filled cushion was placed between the top of the soil sample and top of the chamber to control vertical stress on the soil sample. Ports in the top of the calibration chamber and top cushion allowed cone penetrometers to be pushed into the soil sample.

Baskarp B15 sand and Vingerling K147 clay were used to create the soil models. Baskarp B15 sand classifies as a poorly graded sand (SP) per the Unified Soil Classification System (ASTM [3]) and has a median effective particle diameter (d_{50}) of 0.136 mm, coefficient of uniformity (C_u) of 1.4, coefficient of gradation (C_c) of 1.04, specific gravity (G_S) of 2.65, and maximum and minimum void ratios (e_{max} and e_{min}, respectively) of 0.890 and 0.553. Vingerling K147 clay classifies as lean clay (CL) per the Unified Soil Classification System and has liquid limit (*LL*) of 32.3, plastic limit (*PL*) of 15.8, and a plasticity index (*PI*) of 16.5. The Vingerling K147 clay used to construct the soil models was extruded in a vacuum press, and thus was expected to have a pre-consolidation stress. This was confirmed by the dilative tendencies observed in the stress paths from anisotropic consolidated–undrained (ACU) triaxial compression tests performed on the clay having vertical effective confining stresses of 25 kPa and 50 kPa.

In total, 10 calibration chamber soil models were prepared. Three of these contained pure sand (Models 1, 5, and 6) and serve as reference models and the remainder contained interbedded sand and clay (Models 2, 3, 4, 7, 8, and 10). The model stratigraphies and relevant characteristics are shown in Fig. 2. A complete listing of models and tests performed on them is provided in Appendix A. For the layered soil models, Vingerling K147 clay layers were formed by placing prefabricated clay bricks of the required dimensions into the chamber. The pure sand models and sand layers in the layered models were prepared by water pluviation with a free water height of 1.5–2.5 cm. The density of the sand was closely monitored during the sample preparation by measuring the sample height and weight. The targeted density of the sample was achieved by periodically gently tamping the sand surface during pluviation (van der Linden [51]). Relative densities (D_R) of 30% (loose) and 60% (dense) were targeted; however, as seen in Fig. 2, those target densities were not typically achieved with exact precision during sample preparation. Furthermore, while uncertainty in the D_R was reportedly low for the uniform sand models, uncertainty of D_R in the thin interbedded sands in the layered models was reportedly much greater (De Lange [19]). Local variations in sand density within layers were expected but not anticipated to have a significant impact on the results of this study. For the purposes of this work, it is assumed that the reported D_R is consistent throughout all sand layers in a given soil model. It should be noted that the soil models created for the De Lange [19] study are idealizations of natural soil profiles, with natural soil profiles inherently containing more variability in soil type, soil density/stiffness, layer thickness, etc. and thus being even more difficult to characterize.

The vertical and horizontal stresses confining the soil models were applied via the water pressure in the top cushion and in the annulus between the calibration chamber wall and rubber membrane. The stresses were increased smoothly at a rate of 1 kPa/min until the desired stress levels were reached, where the ratio of horizontal to vertical stress for all tests was 0.5. For the models with clay layers, the clay was allowed to fully consolidate before CPTs were performed.

CPTs were performed through ports in the top plate of the calibration chamber. Two different diameter cones were used in the testing, one having a diameter of 25 mm and the other 36 mm. For the tests where the 36-mm-diameter cone was used, only one CPT was performed on the model and it was pushed down through the center of the model. Accordingly, the cone was 450 mm from the sidewall of the calibration chamber. For the tests where the 25-mm-diameter cone was used, three tests were performed on each model, at the vertices of a centrally positioned equilateral triangle having side lengths of 260 mm. Accordingly, the cones were 300 mm from the sidewall of the calibration chamber for each test, and the confining stress was increased between each test (typically tests were performed at vertical effective confining stresses of 25 kPa, 50 kPa, and 100 kPa). The cones were hydraulically pushed at a rate of 4 mm/s in order to obtain one sample every mm, as the maximum sampling frequency of the data acquisition unit is 4 Hz. Both q_c and sleeve friction (f_s) were measured.

3. Thin-layer correction procedures

Three thin-layer correction procedures are evaluated herein. The first was proposed by Boulanger and DeJong [6] (BD18) and accounts for multiple thin-layer effects by posing the problem as an inverse problem. BD18 assumed that the measured tip resistance (q^m) equals the

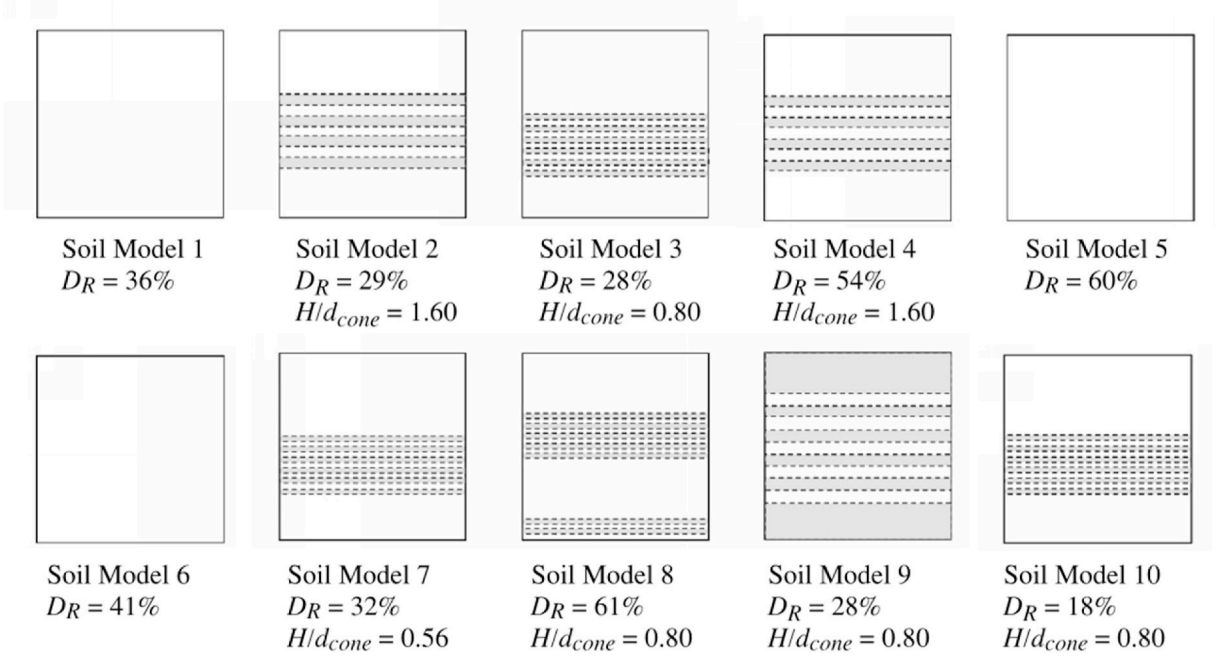

Fig. 2. Stratigraphy, relative density (D_R), and thin layer thickness to cone diameter ratio (H/d_{cone}) of each of the De Lange [14] calibration chamber soil models. The white and gray areas represent the layers of Baskarp B15 sand and Vingerling K147 clay, respectively.

"true" tip resistance (q^t) convolved with a depth-dependent spatial filter (w_c) following a simple 1D model. Additionally, a modified version of the Boulanger and DeJong [6] procedure (i.e., BD18MOD) is also evaluated, with the modifications to the BD18 procedure based on comments provided to the authors by Professor Jason DeJong and geared toward improving the BD18 procedure's thin-layer correction abilities. Finally, A new procedure is proposed herein and is developed by generalizing the trends in the thin-layer effects on q^m predicted by the Koppejan pile capacity method for a known q^t. Because this latter procedure is based on the calibration chamber tests and analyses of the tests performed by Deltares (De Lange [14]), this procedure is referred to as the "Deltares" procedure, as mentioned in the Introduction, even though it was not formally proposed by Deltares.

The following terminology is used in this section:

- q^m – measured tip resistance after corrections for unequal area effects have been applied and normalized to atmospheric pressure
- q^t – true tip resistance (i.e., the tip resistance that would be measured in a given soil layer without any influence of multiple thin-layer effects), normalized to atmospheric pressure
- q^{inv} – tip resistance that when convolved with a depth-dependent spatial filter, best predicts the measured tip resistance per the Boulanger and DeJong [6] inverse procedure (i.e., an estimate of q^t, as detailed herein), normalized to atmospheric pressure
- q^{corr} – corrected tip resistance obtained by applying thin-layer corrections via the Deltares procedure to the measured tip resistance (i.e., an estimate of q^t, analogous to q^{inv} for the BD18 procedure, as detailed herein)

3.1. Overview of the Boulanger and DeJong [6] (BD18) inverse filtering procedure for thin- and transition-layer effects

As mentioned in the Introduction, BD18 proposed an automated procedure to account for multiple thin-layer effects by posing the problem as an inverse problem. They assumed that the measured tip resistance (q^m) equals the "true" tip resistance (q^t) convolved with a depth-dependent spatial filter (w_c) following a simple 1D model:

$$q^m(z) = q^t(z) * w_c(z) \tag{1}$$

where the asterisk indicates convolution of q^t with w_c. In this case, the convolution refers to the integral of the point-wise multiplication of $q^t(z)$ and $w_c(z)$, as a function of the amount that one of the functions is shifted relative to the other.

This technique searches for the "inverted" tip resistance (q^{inv}), that, when convolved with w_c, best predicts q^m, where q^{inv} is an estimate of q^t. The problem is treated as an optimization problem via an iterative splitting method, which seeks to solve:

$$q^{inv} = \underset{q^t}{argmin} \| q^m - q^t * w_c \|_2 \tag{2}$$

with added smoothing and filter procedures to dampen fine-scale features that can be detrimental to convergence. Once the optimization procedure is performed, sharp transitions in q^{inv} are identified. A uniform q^{inv} (either the maximum or minimum q^{inv} identified in the transition zone) is then applied across the entire transition zone. The procedure is described in detail in Appendix B.

The thin-layer factors (K_H) derived from the procedure are shown in Fig. 3, where K_H is defined as:

$$K_H = \frac{q^t(z)}{q^m(z)} \tag{3}$$

where $q^t(z)$ and $q^m(z)$ are the true and measured tip resistances, respectively, at a given depth, z.

In Fig. 3, q^t_{strong} and q^t_{weak} are the values of q^t (or the estimated values of q^t, q^{inv}) in the thin sand and clay layers, respectively, H is the thickness of the thin sand layer, and d_{cone} is the diameter of the cone in the same units as H. As shown in this figure, K_H increases as the normalized thickness, H/d_{cone}, of the thin sand layer decreases, consistent with the trends show in Fig. 1. The thin-layer factor with smoothing and filtering steps included, $K_{H,net}$, decreases as H/d_{cone} approaches zero. The smoothing and filter models are discussed more next.

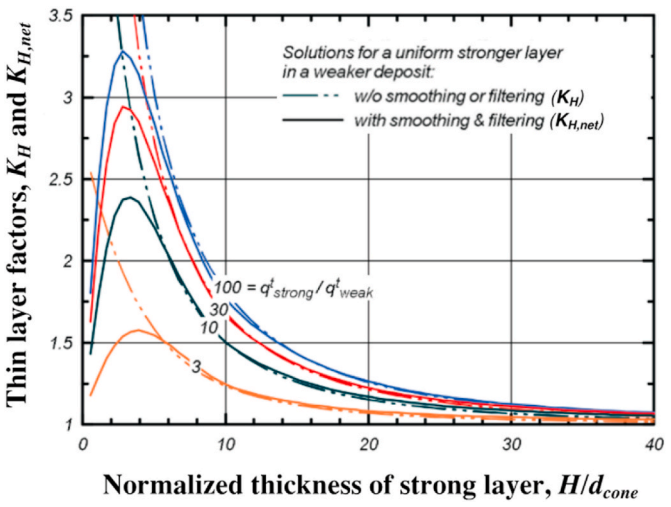

Fig. 3. Thin-layer factors for sand layers derived from the Boulanger and DeJong [6] inversion procedure (BD18) with and without smoothing and filtering (designated as $K_{H,net}$ and K_H, respectively) (Boulanger and DeJong [6]).

3.1.1. Cone penetration filter model

The cone penetration filter model, $w_c(z)$, used by BD18 accounts for the relative influence of soil at a distance from the cone tip (i.e., whether the distant soil is softer or stiffer than the soil immediately adjacent to the cone tip). The cone penetration filter is shown in Fig. 4, normalized by the w_c at the cone tip, as a function of normalized depth, z' (i.e., distance from the cone tip divided by d_{cone}). As shown in this figure, the soil above the cone tip has about half the influence on q^m as compared to the soil below the cone tip, as indicated by the relative areas under the curves. Also, as may be surmised from this figure, if the soil at a given distance from the cone tip is softer than the soil at the cone tip (i.e., $q^t_{z'}/q^t_{z'=0} < 1$), the distant soil will have a larger influence on q^m than it

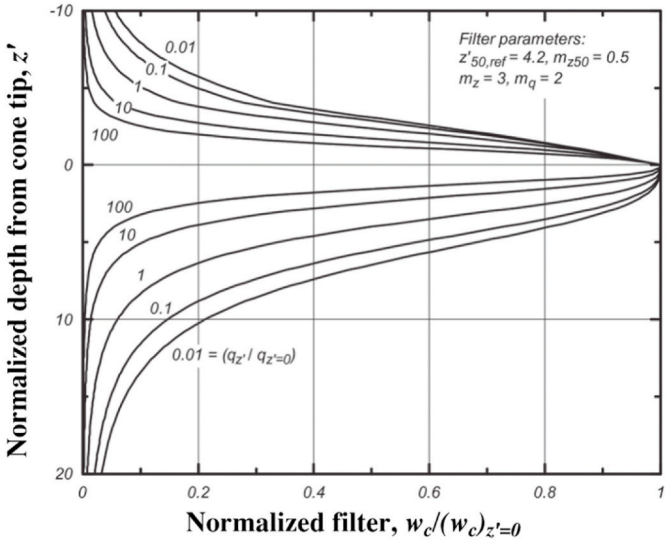

Fig. 4. Normalized cone penetration filter, $w_c/(w_c)_{z'=0}$, vs. normalized depth, z', from the cone tip. (Boulanger and DeJong [6]).

would otherwise, as indicated by the larger area under the curves for decreasing values of $q^t_{z'}/q^t_{z'=0}$.

The cone penetration filter model shown in Fig. 4 has four filter parameters, with baseline values recommended by BD18 for each, which were used in generating Fig. 4 (i.e., $z'_{50,ref} = 4.2$, $m_{z50} = 0.5$, $m_z = 3$, and $m_q = 2$). These parameters can be adjusted to potentially increase or decrease the magnitude of K_H and the sensing and development distances, which may improve identification of very thin layers, but there is no general procedure for automatically determining these parameters.

3.1.2. Smoothing steps in the BD18 procedure

The BD18 inversion procedure includes two steps that decrease K_H as the normalized thin layer thickness (H/d_{cone}) decreases:

1. A smoothing step performed after each iteration of the inversion that first prevents q^{inv} from falling below $0.5q^m$ at any given depth, and second computes a moving average of q^{inv} over a pre-defined smoothing window.
2. The application of a low-pass spatial filter after inversion, which consists of a re-run of the inversion procedure using a limiting $z'_{50,ref}$ value equal to the length of the cone tip, instead of 4.2 that is recommended for the initial inversion.

These steps reportedly improve the performance of the overall procedure and promote convergence of the solution. They also ensure a decrease in K_H as thin layer thickness approaches zero. As shown in Fig. 3, removal of the smoothing and filtering steps causes K_H to approach infinity in very thin layers. However, modifying and removing the smoothing and filtering steps can improve the performance of the inversion procedure in identifying very thin layers, but can also destabilize the solution, resulting in non-convergence as shown in Fig. 5.

In an attempt to improve the performance of the BD18 procedure on the calibration chamber data from Deltares, and at the suggestion of Professor Jason DeJong, the smoothing and filtering steps were both modified and removed from the procedure. The procedure was then implemented to assess the effects of these changes on q^{inv}. Specifically, the following modifications were made to the BD18 procedure:

- Revise the smoothing window used during inversion to cap at a maximum of three q^m data points (note that reducing the window below three q^m data points, or eliminating the smoothing step altogether, results in a solution that does not converge as shown in Fig. 5).
- Revise by reducing the limiting $z'_{50,ref}$ value used in the low-pass spatial filter applied after the inversion, and by eliminating the low-pass spatial filter altogether.
- A combination of reducing the smoothing window and eliminating the low-pass spatial filter that is applied after the inversion.

The combination of reducing the smoothing window and eliminating the low pass spatial filter after inversion produced the best results (as will be discussed subsequently), and is referred to henceforth as BD18MOD.

3.2. Overview of the deltares multiple thin-layer correction procedure

De Lange [14] used the Koppejan method, a Dutch bearing capacity prediction method for piles in stratified profiles, to interpret the trends in the Deltares calibration chamber test data. Specifically, the Koppejan pile capacity method allows q^m to be estimated if q^t is known (i.e., opposite of the issue at hand: estimating q^t for a known q^m). Accordingly, the authors developed the "Deltares" procedure by generalizing the trends in the thin-layer effects on q^m predicted by the Koppejan method for a known q^t.

3.2.1. De Lange [14] K_H curves

De Lange [14] fit the Deltares calibration chamber data with curves predicted by the Koppejan method, as shown in Fig. 6. In this figure, the thin-layer correction factor (K_H) is expressed as a function of the normalized stress ratio (q_{ratio}), which is defined as:

$$q_{ratio} = \frac{q^m_{max} - \sigma_v}{q^m_{min} - \sigma_v} \tag{4}$$

where q^m_{max} and q^m_{min} are the maximum and minimum measured tip resistances, respectively, in the layered zone, and σ_v is the total vertical stress at the depth of interest. Note that De Lange [14] defined K_H per Equation (5), which is slightly different from the BD18 definition.

$$K_H = \frac{q^t - \sigma_v}{q^m_{max} - \sigma_v} \tag{5}$$

The K_H values for the calibration chamber data plotted in this figure were computed as the ratio of tip resistance measured in a reference

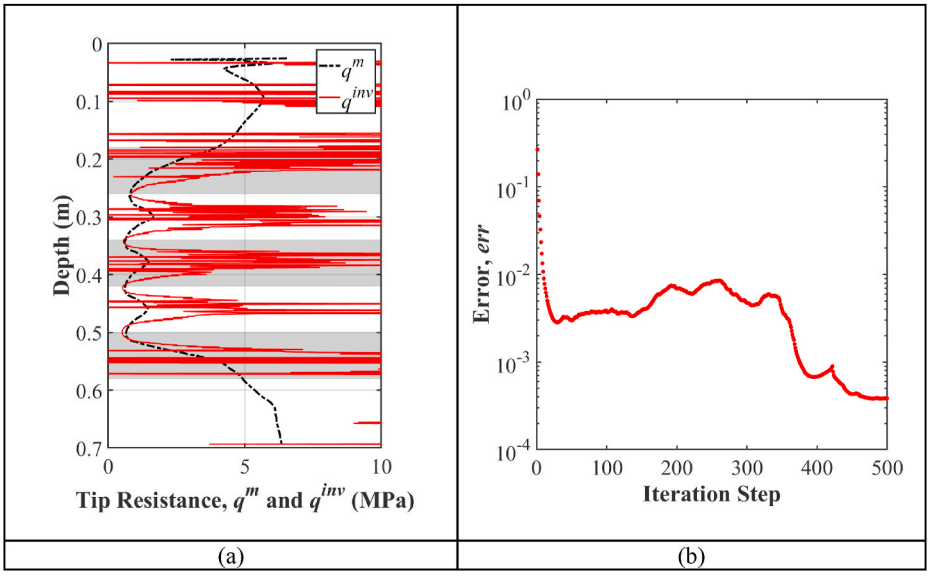

Fig. 5. (a) Unstable results after removal of smoothing procedure from the BD18 procedure as applied to CPT data from the De Lange [14] dataset; and (b) Error plot after removal of the smoothing procedure during inversion. Solution does not converge after 500 steps with $err < 10^{-6}$.

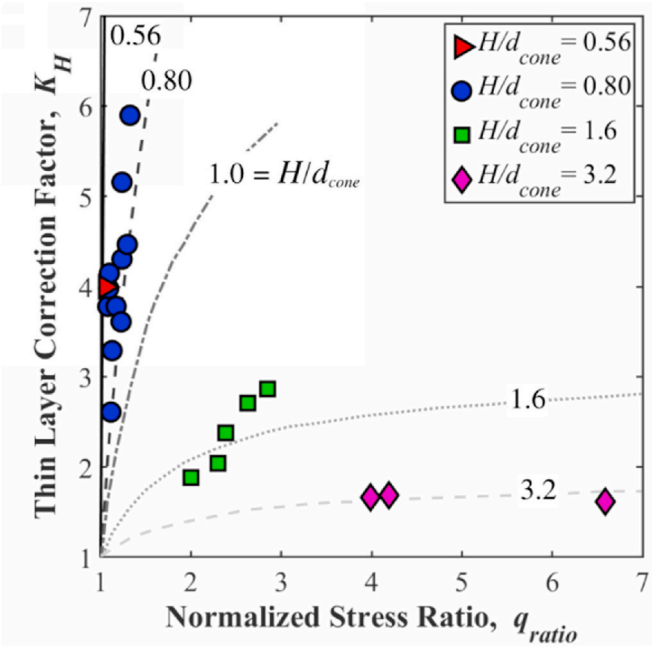

Fig. 6. Thin-layer correction factors (K_H) derived from laboratory test results (shown as points) and numerical simulations using the Koppejan method (shown as curves) (from De Lange [14]).

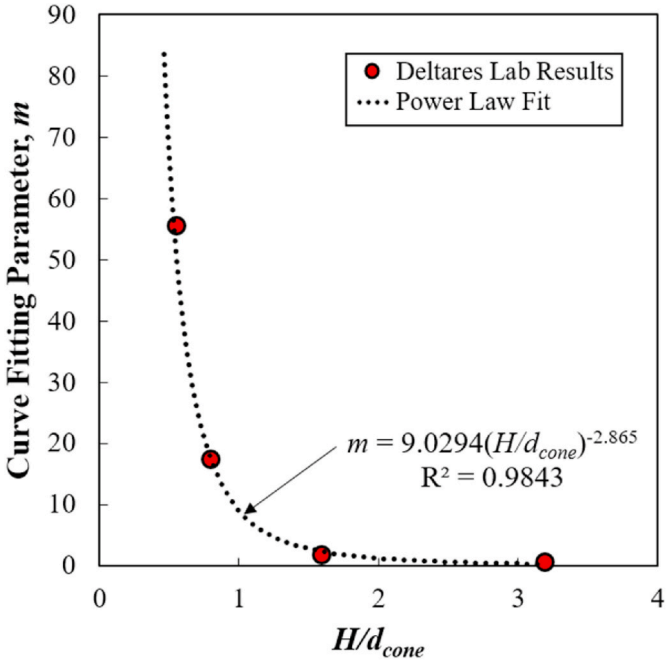

Fig. 7. Relationship between normalized thin layer thickness (H/d_{cone}) and the curve fitting parameter m.

sand model (i.e., q^t) and in the sand layers in a stratified model (i.e., q^m), where the sand in the two models had similar D_R and confining stresses. De Lange [14] showed that K_H is dependent on the thickness of the thin sand layers (H), cone diameter (d_{cone}), sand layer density, and confining stress, and ranged between 1.5 and 6. However, no procedure was explicitly outlined by De Lange [14] on how to calculate thin-layer correction factors for cases where the q^t values are unknown, or for profiles having differing values of normalized layer thickness (i.e., H/d_{cone}) and confining stresses. Additionally, no guidance was provided on implementing the thin-layer correction factors in tandem with transition zone corrections, other than the recommendation that the corrected tip resistance (q^{corr}) be applied over the entire thickness of the thin layer.

The generalization of the trends shown in Fig. 6 and the development of the "Deltares" thin-layer correction procedure are briefly summarized next, and detailed instructions for implementing the procedure are provided in Appendix C.

3.2.2. Derivation of correction factors

In order to calculate K_H for H/d_{cone} and q_{ratio} values other than those reported in De Lange [14], it was necessary to generate a set of curves to fit the calibration chamber data presented in Fig. 6 and to generate additional curves for other H/d_{cone} values. Based on the shape of the Koppejan curves shown in Fig. 6, it was surmised that a logarithmic curve passing through the point (1,1) would reasonably fit the calibration chamber data.

Understanding that the amount of data is limited, logarithmic curves of the form given by Equation (6) were developed to fit the four sets of calibration chamber test data shown in Fig. 6.

$$K_H = m \cdot \ln(q_{ratio}) + 1 \tag{6}$$

A linear regression of K_H versus the natural logarithm of q_{ratio} was used to generate the fitting parameter m. This produced a set of curves that have similar shapes to the Koppejan curves shown in Fig. 6. Additionally, a relationship between the curve fitting parameter m and H/d_{cone} was developed from the calibration chamber data, as shown in Fig. 7.

A power-law fit was used to approximate the relationship shown in Fig. 7. The relationship between H/d_{cone} and the curve fitting parameter m is thus defined by:

$$m = 9.0294\ (H/d_{cone})^{-2.865} \tag{7}$$

Using Equations (6) and (7), curves defining K_H could be generated for any combination of q_{ratio} and H/d_{cone}, as shown in Fig. 8.

Although Equation (6) is an approximation, it can be used to generate K_H values based on q^m values for a variety of thin layer thicknesses, cone diameters, and confining stress. Detailed instructions on

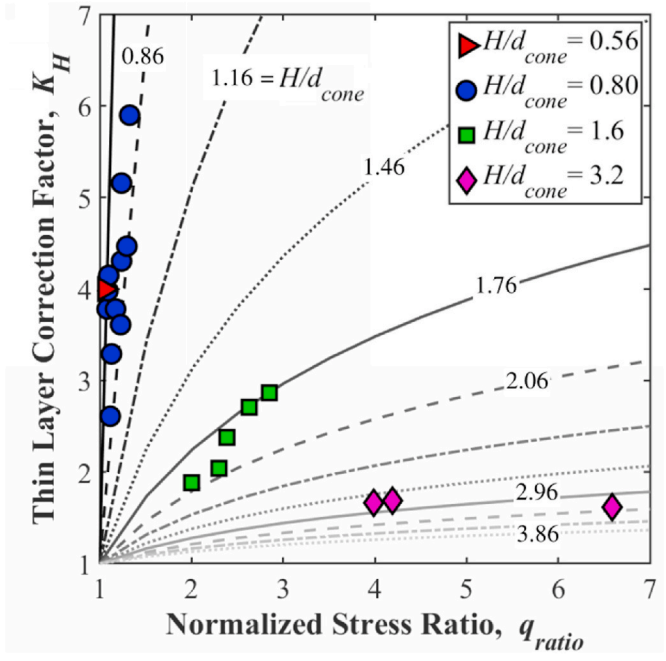

Fig. 8. Thin-layer correction factor (K_H) curves for several normalized thin layer thicknesses (H/d_{cone}) shown as lines and K_H values derived from the calibration chamber tests shown as points.

how to apply the K_H factors to q^m, in tandem with transition layer corrections, to obtain the "corrected" q_c, or q^{corr}, are provided in Appendix C.

4. Application of the thin-layer correction procedures to the calibration chamber data

The BD18, BD18MOD, and Deltares thin-layer correction procedures were applied to the Deltares calibration chamber CPT data to assess their efficacies. However, in comparing the results, it should be remembered that the Deltares procedure was developed and calibrated using the same calibration chamber data that are being used to assess its efficacy, while the BD18 and BD18MOD procedures were calibrated using different data. As a result, the assessment is inherently biased.

Select results from the application of the thin-layer correction procedures are shown in Fig. 9, with the complete results provided in Figure A.1 in Appendix A. In Fig. 9, the black line represents the q^m data, the blue solid line represents q^{inv} from the BD18 procedure, the blue dashed line represents q^{inv} from the BD18MOD procedure (i.e., q^{invmod}), the green dashed line represents q^{corr} from the Deltares procedure, and the red line represents q^t as measured in the corresponding reference sand model (note that q^{inv}, q^{invmod}, and q^{corr} are all estimates of q^t). Reference sand models were selected (from the three CPT soundings performed in uniform sand profiles with the 25-mm-diameter cone in the De Lange [19] dataset) that have a similar D_R and σ'_v to the CPT sounding of interest. Thus, Soil Model 1, CPT 3 ($D_R = 36\%$ and $\sigma'_v = 100$ kPa) is compared to itself [Fig. 9a]; Soil Model 4, CPT 3 ($D_R = 54\%$ and $\sigma'_v = 100$ kPa) and Soil Model 8, CPT 3 ($D_R = 61\%$ and $\sigma'_v = 100$ kPa) are compared to Soil Model 5, CPT 1 ($D_R = 60\%$ and $\sigma'_v = 100$ kPa) [Fig. 9b and c]; and Soil Model 10, CPT 3 ($D_R = 18\%$ and $\sigma'_v = 30$ kPa) is compared to Soil Model 1, CPT 2 ($D_R = 36\%$ and $\sigma'_v = 50$ kPa) [Fig. 9d]. Since none of the reference sand models served as identical comparisons (in terms of σ'_v and D_R of sand) to the layered models, we cannot expect the inverted/corrected results within the sand layers to exactly match the q^t included on the plots in Fig. 9. However, the q^t provides a point of reference indicating the approximate tip resistance magnitude that should be obtained by the inversion/correction procedure over the entire thickness of the thin sand layers in the layered profiles. Observations from the results presented in Fig. 9 are as follows:

- None of the methods perform very well on the reference soil models (i.e., pure sand models: Soil Models 1, 5, and 6), exemplified in Fig. 9a. All procedures erroneously identify and attempt to correct thin layers that were not present. However, the Deltares procedure

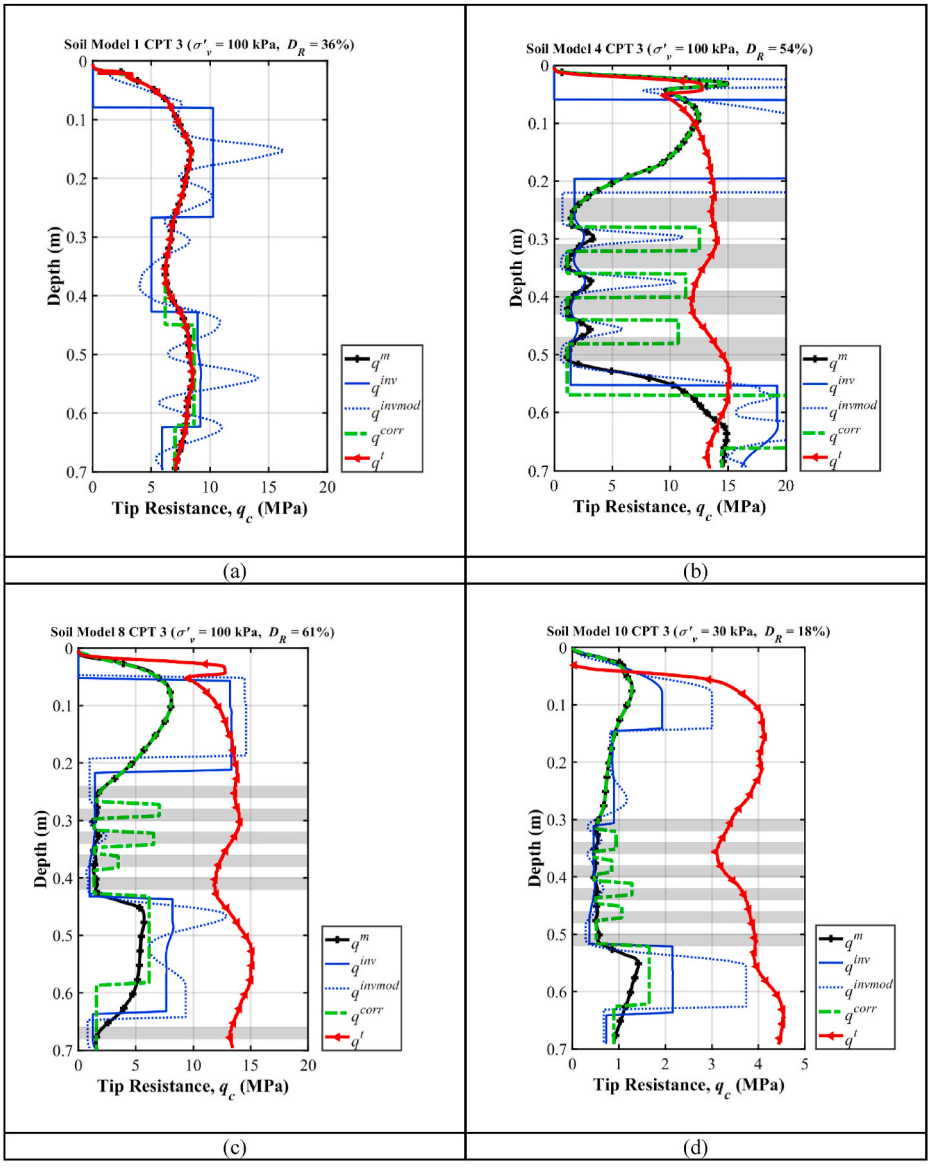

Fig. 9. Results from thin-layer correction procedures applied to: (a) Soil Model 1 (reference soil model - no thin clay layers); (b) Soil Model 4 with 40-mm-thick clay layers represented by the shaded areas; (c) Soil Model 8 with 20-mm-thick clay layers represented by the shaded areas; and (d) Soil Model 10 with 20-mm-thick clay layers represented by the shaded areas, where q^m is measured tip resistance, q^{inv} is the inverted tip resistance per the Boulanger and DeJong (BD18) procedure, q^{invmod} is the inverted tip resistance per the modified BD18 procedure (BD18MOD), q^{corr} is the corrected tip resistance from the Deltares procedure, and q^t is the true tip resistance (as measured in reference sand model).

produces more realistic profiles than the BD18 procedure. The BD18 procedure detects a layer transition if the gradient of q^m with depth falls below a certain value. On the other hand, the Deltares procedure identifies thin layers by using an algorithm that detects local minima (troughs) and maxima (peaks) in q^m. This algorithm can be tuned to filter out peaks and troughs that do not meet minimum prominence criteria to avoid erroneous peak identification. However, it can be very difficult to identify appropriate criteria if the true layering of the soil profile is unknown (which is the case for traditional field CPT data, absent of additional information). This highlights a shortcoming of any thin-layer correction procedure, particularly when applied blindly to field data.

- In the soil models with 40-mm-thick clay layers (Soil Models 2 and 4), the Deltares procedure is effective at identifying the interbedded sand layers and correcting q^m, exemplified in Fig. 9b. In contrast, however, the BD18 procedure actually exacerbates the thin-layer effects, not correcting for them. The modification of BD18 (BD18MOD) results in increased q^{inv} values (i.e., q^{invmod} values) in the thin sand layers and decreased values in the thin clay layers, more consistent with the tip resistances of these layers if they were fully developed.
- Neither the BD18 nor the Deltares procedure are effective in correcting for thin-layer effects when the layers are less than 20 mm thick (i.e., Soil Models 8, 9, and 10), although the Deltares procedure identifies more layers with larger resistance contrasts than the BD18 procedure; refer to Fig. 9c and d. The modifications to BD18 (i.e., BD18MOD) do little to improve the efficacy of the procedure in these specific calibration chamber models. None of the three procedures (Deltares, BD18, or BD18MOD) are able to identify all of the thin layers nor identify the correct layer-boundary locations. However, the efficacies of the procedures are likely limited by the ability of the CPT to accurately detect the presence and location of the layers. For example, variations in q^m in the layered zones of Soil Models 8, 9, and 10 are small relative to measurement noise levels and do not line up well with layer boundaries.
- The modifications to the BD18 procedure (i.e., BD18MOD) eliminate some of the smoothing features inherent to the BD18 procedure and seem to improve the performance of the procedure by increasing the contrast in q^{inv} between the clay and sand for the models with the thicker interbedded layers. However, these modifications also tend to de-stabilize the solution (e.g., see large phantom peak between 0.6 and 0.7 m in Fig. 9b).

It is worthwhile to note that the ratio of stiffness between the sand and clay layers plays a role in the ability of both the CPT and the correction procedures to detect the presence of a thin layer. While De Lange [19] did not report an expected q^t for the clay, a characteristic value of approximately 0.3 MPa can be estimated from Soil Model 9, which had 200-mm-thick clay layers (presumably thick enough for q^t of the clay to develop). Very little increase in q^t of the clay was observed, whereas a very significant increase in q^t of the sand is observed, with increasing confining pressure. In theory, for a given thin-layer thickness, the greater the contrast between the q^t of the sand and the clay, the easier the detection of thin layers will be for both the CPT and the correction procedure. This can be observed when examining the soil models with 40-mm-thick layers, in which, as the confining pressure increases (and consequently the magnitude of the stiffness contrast increases), the difference in magnitude of maximum and minimum q^m in the layered zone increases. However, as layers become thinner (e.g., the soil models with 20-mm-thick layers), the thickness may preclude any notable difference in magnitude of maximum and minimum q^m, despite an increasing stiffness contrast.

5. Application of the thin-layer correction procedures to the CES and Valentine's day earthquake data

The BD18, BD18MOD, and Deltares thin-layer correction procedures were applied to field data from the 2010–2011 CES (i.e., 2010 September M_w 7.1 Darfield and 2011 February M_w 6.2 Christchurch earthquakes) and the 2016 February M_w 5.7 Valentine's Day earthquake that impacted Christchurch, New Zealand. The goal of this effort was to see whether application of the procedures resulted in improved predictions of the actual field liquefaction response. Towards this end, ~3500 CPT soundings from sites where the severity of liquefaction manifestations was well-documented after at least one of the following aforementioned earthquakes were compiled, resulting in ~9150 high quality liquefaction case histories. A detailed description of the selection/rejection criteria for the CPT soundings is provided in Maurer et al. [29,30] and Geyin et al. [17]. The severity of liquefaction manifested at the ground surface was classified in accordance with Green et al. [19] via post-earthquake ground reconnaissance and using high-resolution aerial and satellite imagery. The CPT soundings and imagery used in this study were extracted from the New Zealand Geotechnical Database (NZGD [37]).

5.1. Computation of predicted liquefaction severity

The factor of safety against liquefaction triggering (FS_{liq}) was computed using the CPT-based variant of the simplified procedure proposed by Green et al. [22] (Gea19), in conjunction with peak ground accelerations (*PGA*) estimated following the Bradley [9] procedure, which has been used in many prior studies of these earthquakes (e.g., Green et al. [18,19]; Maurer et al. [29–31]; Carter et al. [10]; among others). However, the case histories associated with the Christchurch earthquake were analyzed using the revised *PGAs* from Upadhyaya et al. [47], which account for the influence of liquefaction on the ground motions recorded by a few strong motions stations. The depth of ground water table immediately prior to each earthquake was estimated using the event-specific regional ground water models of van Ballegooy et al. [49]. An I_c cutoff value of 2.5 was used to distinguish between liquefiable and non-liquefiable soils, where soils with $I_c > 2.5$ were considered to be non-liquefiable (Maurer et al. [33,34]).

The severity of the surficial liquefaction manifestations was predicted using the Liquefaction Potential Index (*LPI*) (Iwasaki et al. [27]). Commonly used *LPI* thresholds for the predicted severity of surficial liquefaction manifestations are (e.g., Maurer et al. [29]): $LPI < 5$ - Minor-to-None; $5 \leq LPI < 15$ - Moderate; and $LPI \geq 15$ - Severe. *LPI* values were computed from the CPT data with and without thin-layer corrections applied, where the "original" and "modified" Boulanger and DeJong [6] (i.e., BD18 and BD18MOD, respectively) and the Deltares thin-layer correction procedures were used.

In general, the resulting *LPI* values computed using the corrected CPT data are only slightly different from those computed using the uncorrected CPT data. *LPI* values across the database, in general, are reduced as a result of the corrections (i.e., less severe surficial liquefaction manifestations are predicted). The decrease is most significant for the BD18MOD procedure, followed by the BD18 and the Deltares procedures, respectively.

5.2. ROC analyses

To assess the efficacies of the thin-layer correction procedures, the case histories were parsed into bins of I_{c10}, and receiver-operating-characteristic (ROC) analyses (e.g., Fawcett [16]) were performed on each I_{c10} data bin. ROC analyses are commonly used to evaluate the performance of diagnostic models and have been used extensively in medical diagnostics (e.g., Zou [56]) and to a much lesser degree in geotechnical engineering (e.g., Oommen et al. [38]; Maurer et al. [30,32,33]; Green et al. [21]; Zhu et al. [55]; Upadhyaya et al. [48]). In any

ROC analysis application, the distribution of "positives" (e.g., cases of observed surficial liquefaction manifestations) and "negatives" (e.g., cases of no observed surficial liquefaction manifestations) overlap when the frequency of the distributions are expressed as a function of the diagnostic test results (e.g., *LPI* values). A ROC curve can be drawn by plotting the True Positive Rate (R_{TP}) (e.g., liquefaction is predicted and manifestations were observed) versus the False Positive Rate (R_{FP}) (e.g., liquefaction is predicted but no manifestations were observed) for varying threshold values (e.g., threshold *LPI* values). A conceptual illustration of ROC analysis is shown in Fig. 10, including the relationship among the positive and negative distributions, the threshold *LPI* values, and the ROC curve.

In ROC-curve space, a random guess is indicated by a 1:1 line through the origin, while a perfect model plots along the left vertical and upper horizontal axes, connecting at point (0,1). A perfect model indicates the existence of a threshold value that perfectly segregates the dataset (e.g., a threshold *LPI* value below which all the cases are "no manifestation" and above which all the cases are "manifestation"). The area under the ROC curve (*AUC*) can be used as an index to evaluate the predictive performance of a diagnostic test (e.g., correlation of computed *LPI* values using CPT data with thin layer corrections applied per BD18 to observed severity of surficial liquefaction manifestations) whereby higher *AUC* indicates better predictive capabilities. *AUC* is statistically equivalent to the probability that sites observed to have liquefaction surface manifestations have higher *LPI* values than sites observed to have no surface manifestations (Fawcett [16]). As such, a random guess returns an *AUC* of 0.5 whereas a perfect model returns an *AUC* of 1, as illustrated in Fig. 10b. Specific to this study, the efficacies of the thin-layer correction procedures are assessed by comparing the *AUC* values corresponding to uncorrected versus corrected CPT data, where the BD18, BD18MOD, and Deltares procedures are used to correct the CPT data for thin-layer effects.

5.3. Results

Table 1 summarizes the results of the ROC analyses for different severities of surficial liquefaction manifestations for all the cases histories grouped together, and for when the case histories are parsed into bins of $I_{c10} < 2.05$ and $I_{c10} \geq 2.05$. Recall that the deposits in eastern Christchurch predominantly have an $I_{c10} < 2.05$ and those in western Christchurch predominantly have an $I_{c10} > 2.05$, where the profiles with an $I_{c10} > 2.05$ were shown to be highly stratified. The severity of liquefaction during the CES and Valentine's Day earthquake was severely-to-excessively over-predicted (i.e., predicted *LPI* was 10–15 points greater than the expected *LPI* for a given liquefaction damage classification, per criteria presented in Maurer et al. [29]) for this latter set of profiles using the uncorrected CPT data (e.g., Maurer et al. [29]; van Ballegooy et al. [50]; Beyzaei et al. [4]; Stringer et al. [46]; McLaughlin [35]; Beyzaei et al. [5]; Cox et al. [13]; among others). Accordingly, if a thin-layer correction procedure is effective, the *AUC* value is expected to increase when the procedure is applied to the CPT data, especially the *AUC* value for the case histories that have $I_{c10} > 2.05$ (i.e., highly stratified profiles).

Table 1
Summary of the results from the ROC analyses obtained using the uncorrected and corrected CPT data using the BD18, BD18MOD, and Deltares procedures for all the case histories and for bins of cases histories having $I_{c10} < 2.05$ and $I_{c10} \geq 2.05$ (highest values of *AUC* within an I_{c10} bin are bolded and italicized).

Manifestation Severity (Green et al. [19])	Inversion Procedure	I_{c10}		
		All	<2.05	≥2.05
		AUC	AUC	AUC
Any manifestation	Uncorrected	0.8314	0.8594	***0.7633***
	BD18	0.8325	0.8628	0.7565
	BD18 Mod	***0.8356***	***0.8660***	0.7591
	Deltares	0.8295	0.8598	0.7600
Marginal	Uncorrected	0.7798	0.8013	0.7115
	BD18	0.7827	0.8065	0.7089
	BD18 Mod	***0.7856***	***0.8108***	0.7105
	Deltares	0.7780	0.8011	***0.7116***
Moderate	Uncorrected	***0.6577***	0.6880	***0.6387***
	BD18	0.6524	0.6884	0.6178
	BD18 Mod	0.6554	0.6899	0.6201
	Deltares	0.6530	***0.6901***	0.6208
Severe	Uncorrected	0.7100	0.6912	0.7602
	BD18	0.7098	0.6895	0.7665
	BD18 Mod	***0.7120***	0.6914	***0.7696***
	Deltares	0.7116	***0.6932***	0.7614

From examination of the *AUC* values listed in Table 1, an increasing trend in *AUC* for the corrected CPT data is not observed. Rather, the *AUC* values do not vary much for the uncorrected versus corrected CPT data. Moreover, the *AUC* values are generally slightly higher for the uncorrected CPT data for case histories having $I_{c10} > 2.05$ than when the CPT data is corrected for thin-layer effects (i.e., exactly opposite of what would be expected if the thin-layer corrections were effective). Because the analysis of the calibration chamber data showed that none of the procedures were able to accurately identify and characterize layers that

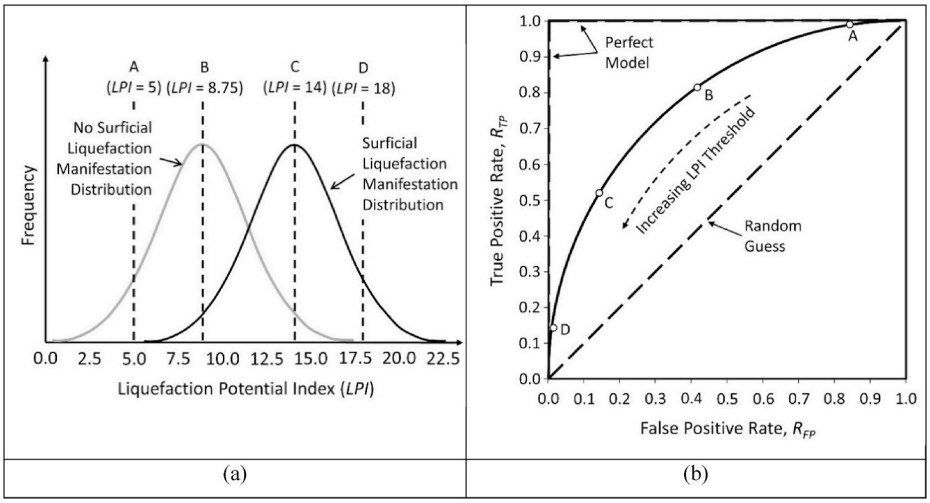

Fig. 10. Conceptual illustration of ROC analyses: (a) frequency distributions of liquefaction manifestation and no liquefaction manifestation observations as a function of *LPI*; (b) corresponding ROC curve, where the area under the ROC curve (*AUC*) is used to assess the efficiency of a diagnostic test (after Maurer et al. [30,31]).

are 20–40 mm thick, the lack of clearly increased AUC after correction is unsurprising.

6. Discussion and conclusions

The BD18/BD18MOD and the Deltares procedures are fundamentally different approaches to correcting data. The Deltares procedure is an algorithm to enhance existing peaks and troughs after smoothing the measured data, and is designed to require outputs to appear as clear layers for easier stratigraphic interpretation of the inverted models. It is not an inverse problem approach, because it does not predict what data would be measured for the proposed q^{corr} model for comparison to the measured data q^{m} as is done by the BD18 and BD18MOD procedures (which are inverse problem approaches). Because the Deltares procedure was developed based on calibrations of only a few laboratory datasets, while the BD18 and BD18MOD include general steps to better model any data acquired, one might expect more general utility of BD18 and BD18MOD across a broader range of stratigraphy scenarios. However, all procedures struggled with detection of fine layers, as noted above. While the basic iterative splitting scheme underlying BD18 and BD18MOD would be expected to converge to a model that minimizes the measured-versus-predicted data misfit when compared to slightly different models, we have no guarantees that this model is a global minimizer of this data misfit over all models. Rather, the resulting model could be a local minimizer, meaning it is simply the best model compared to a small group of similar models, which is a fundamental challenge in inverse problems. Further study is needed to understand the potential for local minimizers in this problem, as well as to use optimization regularization to push the iterative search towards physically realistic stratigraphy that better explains the measured data.

As presented above, calibration chamber data (De Lange [14]) was used to assess the efficacy of the BD18, BD18MOD, and Deltares procedures, although this was not a true test of the Deltares procedure's efficacy because that procedure was developed and calibrated using these same calibration chamber data. Nevertheless, the results of these efforts showed that the BD18 procedure was not able to accurately identify and characterize layers that are 40 mm thick (or less), and actually numerically smoothed the measured CPT data, opposite of its intent. Modifying the BD18 procedure by reducing the smoothing window and eliminating the low pass spatial filter after inversion (BD18MOD) improved the ability of the procedure to identify and characterize layers that were 40 mm thick, however, the modified procedure was still not able to accurately identify and characterize layers that were 20 mm thick. The Deltares procedure did a good job identifying and characterizing layers that were 40 mm thick, but its efficacy was also not good for 20-mm-thick layers.

The BD18, BD18MOD, and Deltares procedures were used to analyze case histories from the 2010–2011 CES and the 2016 Valentine's Day earthquake with and without the application of the thin-layer corrections to the CPT data. The results showed that the thin-layer corrections generally resulted in slightly less accurate predictions of the liquefaction severity for cases having highly stratified profiles, opposite of what would be expected and desired. However, limitations in the thin-layer correction procedures may only be one reason for this trend. For example, the applied procedures could be appropriately correcting CPT tip resistance for thin-layer effects, but shortcomings in the liquefaction triggering and manifestation models could still prevent the accurate predictions of cumulative liquefaction response of the profiles. As a result, the observed trends in accuracy of liquefaction severity prediction provide evidence that the thin-layer corrections do not improve predictions using existing liquefaction models, but not direct evidence that the thin-layer corrections are not efficacious unto themselves.

In addition to potential limitations in the triggering and manifestation models, the depth interval for the Canterbury CPT q_c measurements was 1 and 2 cm; specifically, the interval was 1 cm for 5485 of the case histories analyzed and 2 cm for 3668 of the case histories. These measurement intervals are on par with the thicknesses of the thin layers identified in many of the western Christchurch profiles (Beyzaei et al. [5]). As a result, many of the thin layers in the profiles are only being characterized by one or two q_c measurements, if at all. Even the most efficacious thin-layer correction procedure may not be effective under these conditions, particularly if no q_c measurements are made in the thin layer or if the one or two q_c measurements made in a thin layer are "noisy." [Note that this was not an issue with the Deltares calibration chamber tests presented above because the q_c measurements were made using a depth interval of only 1 mm. As a result, approximately 20 q_c measurements were made in the thinnest layers.]

Finally, per the liquefaction triggering model used (as well as most other CPT-based liquefaction triggering models), the liquefaction susceptibility of a layer is based on the Soil Behavior Type Index (I_c), which is a function of both the CPT q_c and sleeve friction (f_s). The main focus of the study presented herein is on thin-layer effects on q_c, but thin-layer effects also affect f_s and in a more complex way than they affect q_c. In addition to the stress-bulb-influence-zone phenomenon that influences the measured q_c (i.e., the main focus of the study presented herein), f_s thin-layer effects entail two other phenomena. First is the physical length of the friction sleeve relative to the thickness of the thin layers. Friction sleeves typically have a surface area of 15,000 mm^2, and as a result, the length of the friction sleeve will vary depending on the diameter of the cone (e.g., Saussus et al. [42]). Most of the CPT soundings performed in Canterbury had projected cross-sectional areas of 10 or 15 cm^2, implying that the friction sleeves were 133.7-mm or 109.3-mm long, respectively. Accordingly, potentially several thin layers were in contact with the friction sleeve for the Canterbury CPT soundings while the cone tip was at any given depth, making the quantification of any given layer's contribution to the measured f_s difficult to discern. The ambiguity in a thin layer's contribution to the measured f_s is furthered as a result of the soil in an overlying layer being "dragged down" into the underlying layer by the cone as it advances in depth. This latter phenomenon was clearly noted in the post-test, excavated calibration chamber samples performed by Deltares (van der Linden [51]; De Lange [14]).

Errors in properly characterizing the f_s of a layer inherently influences the accuracy of predicted liquefaction susceptibility and potential of the layer. While the BD18, BD18MOD, and Deltares procedures apply a correction for the stress-bulb-influence-zone phenomenon on the measured f_s, they do not correct for the effects of multiple-layer-contact and layer down-drag on the measured f_s, which may be significant. [Note that there was no recommendation included in De Lange [14] for correcting or adjusting the measured f_s for thin layer effects. However, the measured f_s was computed herein as part of the "Deltares" procedure using the same procedure used in the BD18 method (as described in *Part 2: Inversion for Sleeve Friction* of Appendix B), except that q^{corr} was used instead of q^{inv}.]

In conclusion, while current procedures for correcting for thin-layer effects are a step in the right direction, they are not sufficient for use with profiles that have layers thinner than 20–40 mm, such as the profiles in western Christchurch, New Zealand, the Flaser bed deposits or tidal flats in the Groningen region of the Netherlands, and similar deposits worldwide. In addition to reducing the depth interval for q_c measurements (i.e., increasing the sampling frequency), one potential way to better identify and characterize thin layers is by using a Vision Cone Penetrometer (VisCPT) (Hryciw et al. [24]). The third generation VisCPT is now under development (Ventola et al. [52]) and will feature enhanced image acquisition. The VisCPT window near the cone tip may allow direct imaging of thin layers and/or the identification of the occurrence and the extent of layer down-drag. This additional information, coupled with more robust inversion algorithms (e.g., Cooper et al. [12]), may lead to a more accurate approach for correcting for thin-layer effects.

Data availability statement

Some or all data, models, or code that support the findings of this study are available from the corresponding author upon reasonable request.

CRediT authorship contribution statement

Kaleigh M. Yost: Data curation, Formal analysis, Investigation, Methodology, Software, Validation, Writing – original draft, Writing – review & editing. **Russell A. Green:** Conceptualization, Funding acquisition, Investigation, Methodology, Project administration, Resources, Supervision, Validation, Writing – original draft, Writing – review & editing. **Sneha Upadhyaya:** Data curation, Formal analysis, Software, Writing – review & editing. **Brett W. Maurer:** Data curation, Formal analysis, Software, Writing – review & editing. **Alba Yerro-Colom:** Investigation, Methodology, Project administration, Resources, Software. **Eileen R. Martin:** Investigation, Methodology, Project administration, Resources, Software, Writing – review & editing. **Jon Cooper:** Formal analysis, Software.

Declaration of competing interest

The authors declare that they have no known competing financial interests or personal relationships that could have appeared to influence the work reported in this paper.

Acknowledgements

This research was partially funded by Nederlandse Aardolie Maatschappij B.V. (NAM) and National Science Foundation (NSF) Grant Numbers CMMI-1825189 and CMMI-1937984. This support is gratefully acknowledged. Additionally, the motivation for this paper came primarily from discussions related to liquefaction hazard due to induced earthquakes in the Groningen gas field in the Netherlands. We thank Julian Bommer, Imperial College London, and Jan van Elk, NAM, as well as all the individuals from NAM, Shell, and Deltares for the discussions that both prompted and informed our efforts to investigate thin layer effects. Additionally, particular thanks are due to Peter Robertson, Gregg Drilling & Testing, Inc., for commenting on the paper, and to Jason DeJong, UC Davis, M. Geyin, University of Washington, and Sjoerd van Ballegooy, Tonkin + Tayler, for discussions about the implementation and modification of the BD18 procedure. However, any opinions, findings, and conclusions or recommendations expressed in this material are those of the authors and do not necessarily reflect the views of NAM or NSF, or those who inspired this work.

Appendix A. Supplementary data

Supplementary data to this article can be found online at https://doi.org/10.1016/j.soildyn.2021.106677.

References

[1] Ahmadi MM, Robertson PK. Thin-layer effects on CPT qc measurement. Can Geotech J 2005;42:1302–17.
[2] Andrus RD, Stokoe II KH. Guide for shear-wave-based liquefaction potential evaluation. Earthq Spectra 2004;20(2):285–305.
[3] ASTM. Standard practice for classification of soils for engineering purposes (unified soil classification System), D2vols. 487–17. West Conshohocken, PA: ASTM International; 2017.
[4] Beyzaei CZ, Bray JD, Cubrinovski M, Riemer M, Stringer ME, Jacka M, Wentz FJ. Liquefaction resistance of silty soils at the Riccarton Road site, Christchurch, New Zealand. In: Proc. 6th int. Conf. Earthquake geotech. Eng; 2015. Paper No. 616.
[5] Beyzaei CZ, Bray JD, van Ballegooy S, Cubrinovski M, Bastin S. Swamp depositional environmental effects on liquefaction performance in Christchurch, New Zealand. In: Proc. 3rd intern. Conf. On performance-based design in earthquake geotechnical engineering (PBDIII), vancouver, Canada, 16-19 july; 2017.
[6] Boulanger RW, DeJong JT. Inverse filtering procedure to correct cone penetration data for thin-layer and transition effects. In: Cone penetration testing 2018. CRC Press; 2018. p. 25–44.
[7] Boulanger RW, Idriss IM. CPT and SPT based liquefaction triggering procedures. Report No. UCD/CGM-14/01. Davis, CA: Center for Geotechnical Modeling, Department of Civil and Environmental Engineering, University of California; 2014. p. 134.
[8] Boulanger RW, Moug DM, Munter SK, Price AB, DeJong JT. Evaluating liquefaction and lateral spreading in interbedded sand, silt and clay deposits using the cone penetrometer. Aust GeoMech 2016;51(4):109–28.
[9] Bradley BA. Site-Specific and spatially-distributed ground motion intensity estimation in the 2010-2011 Christchurch earthquakes. Soil Dynam Earthq Eng 2013;48:35–47.
[10] Carter WL, Green RA, Bradley BA, Wotherspoon LM, Cubrinovski M. Spatial variation of magnitude scaling factors during the 2010 Darfield and 2011 Christchurch, New Zealand, earthquakes. Soil Dynam Earthq Eng 2016;91:175–86.
[11] Cetin KO, Seed RB, Der Kiureghian A, Tokimatsu K, Harder LF, Kayen RE, Moss RES. Standard penetration test-based probabilistic and deterministic assessment of seismic soil liquefaction potential. J Geotech Geoenviron Eng 2004;130(12):1314–40.
[12] Cooper J, Martin E, Yost K, Yerro-Colom A, Green RA. Robust identification and characterization of thin soil layers in cone penetration data by piecewise layer optimization. Comput Geotech 2021. Submitted for publication.
[13] Cox BR, McLaughlin KA, van Ballegooy S, Cubrinovski M, Boulanger RW, Wotherspoon L. In-situ investigations of false-positive liquefaction sites in Christchurch, New Zealand: st. Teresa's school case history. In: *Proc. 3rd intern. Conf. On performance-based Design in earthquake geotechnical engineering* (PBDIII), vancouver, Canada, 16-19 july; 2017.
[14] De Lange DA. In: van Elk J, Doornhof D, editors. CPT in thinly layered soils. Delft, the Netherlands: Deltares; 2018.
[15] El Kortbawi M, Green RA, Wotherspoon L, van Ballegooy S. Insights into the liquefaction hazard in napier and hastings based on the assessment of data from the 1931 Hawke's Bay, New Zealand, earthquake. In: *Proc. 13th Australia New Zealand Conference on geomechanics* (13ANZCG), perth, Australia, 1-3 april; 2019.
[16] Fawcett T. An introduction to ROC analysis. Pattern Recogn Lett 2006;27(8):861–74.
[17] Geyin M, Maurer BW, Bradley BA, Green RA, van Ballegooy S. CPT-based liquefaction case histories compiled from three earthquakes in Canterbury, New Zealand. Data paper. Earthq Spectra 2021. In press.
[18] Green RA, Allen J, Wotherspoon L, Cubrinovski M, Bradley B, Bradshaw A, Cox B, Algie T. Performance of levees (stopbanks) during the 4 september 2010, M_w7.1 Darfield and 22 february 2011, M_w6.2 Christchurch, New Zealand earthquakes. Seismol Res Lett 2011;82(6):939–49.
[19] Green RA, Cubrinovski M, Cox B, Wood C, Wotherspoon L, Bradley B, Maurer BW. Select liquefaction case histories from the 2010-2011 Canterbury earthquake sequence. Earthq Spectra 2014;30(1):131–53.
[20] Green RA, Maurer BW, Cubrinovski M, Bradley BA. Assessment of the relative predictive capabilities of CPT-based liquefaction evaluation procedures: lessons learned from the 2010-2011 Canterbury earthquake sequence. In: *Proc. 6th intern. Conf. On earthquake geotechnical engineering* (6ICEGE), Christchurch, New Zealand, 2-4 november; 2015.
[21] Green RA, Upadhyaya S, Wood CM, Maurer BW, Cox BR, Wotherspoon L, Bradley BA, Cubrinovski M. Relative efficacy of CPT- versus Vs-based simplified liquefaction evaluation procedures. In: *Proc. 19th intern. Conf. On soil Mechanics and geotechnical engineering*, Seoul, Korea, 17-22 September; 2017.
[22] Green RA, Bommer JJ, Rodriguez-Marek A, Maurer B, Stafford P, Edwards B, Kruiver PP, de Lange G, van Elk J. Addressing limitations in existing 'simplified' liquefaction triggering evaluation procedures: application to induced seismicity in the groningen gas field. Bull Earthq Eng 2019;17(8):4539–57.
[23] Green RA, Bommer JJ, Stafford PJ, Maurer BW, Kruiver PP, Edwards B, Rodriguez-Marek A, de Lange G, Oates SJ, Storck T, Omidi P, Bourne SJ, van Elk J. Liquefaction hazard in the groningen region of The Netherlands due to induced seismicity. J Geotech Geoenviron Eng 2020;146(8). 04020068.
[24] Hryciw RD, Jung Y, Susila E, Ibrahim A. Thin soil layer detection by VisCPT and FEM simulations. In: Proc. 7th intern. Conf. On soil *Mechanics and geotechnical engineering* (ICSMGE), alexandria, Egypt. IOS Press; 2009. p. 1052–5.
[25] Idriss IM, Boulanger RW. Semi-empirical procedures for evaluating liquefaction potential during earthquakes. Journal of Soil Dynamics and Earthquake Engineering 2006;26:115–30.
[26] Idriss IM, Boulanger RW. Soil liquefaction during earthquakes, Monograph MNO-12. Oakland, CA: Earthquake Engineering Research Institute; 2008. p. 261.
[27] Iwasaki T, Tatsuoka F, Tokida K, Yasuda S. A practical method for assessing soil liquefaction potential based on case studies at various sites in Japan. *Proc. 2nd intern. Conf. On Microzonation,* nov 26-dec 1 1978, san Francisco, CA, USA.
[28] Kayen RE, Moss RES, Thompson EM, Seed RB, Cetin OK, Der Kiureghian A, Tanaka Y, Tokimatsu T. Shear wave velocity-based probabilistic and deterministic assessment of seismic soil liquefaction potential. J Geotech Geoenviron Eng 2013;139(3):407–19.
[29] Maurer BW, Green RA, Cubrinovski M, Bradley BA. Evaluation of the liquefaction potential index for assessing liquefaction hazard in Christchurch, New Zealand. J Geotech Geoenviron Eng 2014;140(7). 04014032.
[30] Maurer BW, Green RA, Cubrinovski M, Bradley B. Fines-content effects on liquefaction hazard evaluation for infrastructure during the 2010-2011 Canterbury, New Zealand earthquake sequence. Soil Dynam Earthq Eng 2015;76:58–68.

[31] Maurer BW, Green RA, Cubrinovski M, Bradley B. Assessment of CPT-based methods for liquefaction evaluation in a liquefaction potential index framework. Geotechnique 2015;65(5):328–36.
[32] Maurer BW, Green RA, van Ballegooy S, Bradley BA, Upadhyaya S. Performance comparison of probabilistic and deterministic liquefaction triggering models for hazard assessment in 23 global earthquakes. In: Huang J, Fenton GA, Zhang L, Griffiths DV, editors. Geo-Risk 2017: reliability-based design and code developments, vol. 283. ASCE Geotechnical Special Publication; 2017. p. 31–42.
[33] Maurer BW, Green RA, van Ballegooy S, Wotherspoon L. Assessing liquefaction susceptibility using the CPT soil behavior type index. In: *Proc. 3rd intern. Conf. On performance-based Design in earthquake geotechnical engineering* (PBDIII), vancouver, Canada, 16-19 july; 2017.
[34] Maurer BW, Green RA, van Ballegooy S, Wotherspoon L. Development of region-specific soil behavior type index correlations for evaluating liquefaction hazard in Christchurch, New Zealand. Soil Dynam Earthq Eng 2019;117:96–105.
[35] McLaughlin KA. Investigation of false-positive liquefaction case history sites in Christchurch, New Zealand. MS Thesis. Austin, TX: Department of Civil, Architectural, and Environmental Engineering, University of Texas at Austin; 2017. p. 156.
[36] Moss RES, Seed RB, Kayen RE, Stewart JP, Der Kiureghian A, Cetin KO. CPT-based probabilistic and deterministic assessment of in situ seismic soil liquefaction. J Geotech Geoenviron Eng 2006;132(8):1032–51.
[37] NZGD. New Zealand geotechnical database. Earthquake Commission (EQC), New Zealand, https://www.nzgd.org.nz/Default.aspx. [Accessed 24 August 2016].
[38] Oommen T, Baise LG, Vogel R. Validation and application of empirical liquefaction models. J Geotech Geoenviron Eng 2010;136(12):1618–33.
[39] Robertson PK. Soil classification using the cone penetration test. Can Geotech J 1990;27(1):151–8.
[40] Robertson PK, Fear CE. Liquefaction of sands and its evaluation. *Keynote lecture*. In: Ishihara K, editor. *IS Tokyo '95, proc. 1st intern. Conf. Earthquake geotechnical engineering*. Amsterdam: A.A. Balkema; 1995.
[41] Robertson PK, Wride CE. Evaluating cyclic liquefaction potential using the cone penetration test. Can Geotech J 1998;35(3):442–59.
[42] Saussus DR, Frost JD, DeJong JT. Statistical analysis of friction sleeve length effects on soil classification. Int J Numer Anal Methods GeoMech 2004;28:1257–78.
[43] Seed HB, Idriss IM. Simplified procedure for evaluating soil liquefaction potential. J Soil Mech Found Div 1971;95(5):1199–218.
[44] Seed HB, Tokimatsu K, Harder LF, Chung RM. Influence of SPT procedures in soil liquefaction resistance evaluations. Journal of Geotechnical Engineering 1985;111(2):1425–45.
[45] Stark TD, Olson SM. Liquefaction resistance using CPT and field case histories. Journal of Geotechnical Engineering 1995;121(12):856–69.
[46] Stringer M, Beyzaei C, Cubrinovski M, Bray J, Riemer M, Jacka M, Wentz F. Liquefaction characteristics of Christchurch silty soils: gainsborough reserve. In: Proc. 6th int. Conf. Earthquake geotech. Eng; 2015. Paper No. 726.
[47] Upadhyaya S, Green RA, Rodriguez-Marek A, Maurer BW, Wotherspoon L, Bradley BA, Cubrinovski M. Influence of corrections to recorded peak ground accelerations due to liquefaction on predicted liquefaction response during the 2010-2011 Canterbury, New Zealand, earthquake sequence. In: *13th Australia New Zealand conf. On geomechanics* 2019; April 1-3 2019. Perth, Australia.
[48] Upadhyaya S, Maurer BW, Green RA, Rodriguez-Marek A. Selecting optimal factor of safety and probability of liquefaction triggering thresholds for engineering projects based on misprediction costs. J Geotech Geoenviron Eng 2021. https://doi.org/10.1061/(ASCE)GT.1943-5606.0002511.
[49] van Ballegooy S, Cox SC, Thurlow C, Rutter HK, Reynolds T, Harrington G, et al. Median water table elevation in Christchurch and surrounding area after the 4 September 2010 Darfield earthquake: version 2. GNS Science Report 2014/18, 79 pages plus 8 appendices. 2014.
[50] van Ballegooy S, Malan P, Lacrosse V, Jacka ME, Cubrinovski M, Bray JD, O'Rourke TD, Crawford SA, Cowan H. Assessment of liquefaction-induced land damage for residential Christchurch. Earthq Spectra 2014;30(1):31–55.
[51] van der Linden TI. Influence of multiple thin soft layers on the cone resistance in intermediate soils. MS Thesis. Delft, the Netherlands: Delft University of Technology; 2016.
[52] Ventola A, Dolling R, Hryciw RD. Image analysis and hardware developments for the vision cone penetrometer. In: ASCE GeoCongress; 2020. p. 640–8. Geotechnical Special Publication 317.
[53] Whitman RV. Resistance of soil to liquefaction and settlement. Soils Found 1971;11(4):59–68.
[54] Youd TL, Idriss IM, Andrus RD, Arango I, Castro G, Christian JT, Dobry R, Finn WDL, Harder LF, Hynes ME, Ishihara K, Koester JP, Liao SSC, Marcuson III WF, Martin GR, Mitchell JK, Moriwaki Y, Power MS, Robertson PK, Seed RB, Stokoe II KH. Liquefaction resistance of soils: summary report from the 1996 NCEER and 1998 NCEER/NSF workshops on evaluation of liquefaction resistance of soils. J Geotech Geoenviron Eng 2001;127(4):297–313.
[55] Zhu J, Baise LG, Thompson EM. An updated geospatial liquefaction model for global application. Bull Seismol Soc Am 2017;107(3). https://doi.org/10.1785/0120160198.
[56] Zou KH. Receiver operating characteristic (ROC) literature research. On-line bibliography available from: http://www.spl.harvard.edu/archive/spl-pre2007/pages/ppl/zou/roc.html. [Accessed 10 March 2016].